ISSN: 2710-0723

Erosion Behavior and Surface Strengthening of Hydraulic Cylinders

Wenjun Wang[1,2], Aili Li[1,2,*], Gang Liao[1,2], Tianzhou Li[3]

[1] National Engineering Research Center for Oil&Gas Drilling Equipment, Baoji 721002, China

[2] Baoji Oilfield Machinery Co., Ltd, Baoji 721002, China

[3] School of Mechatronic Engineering, Southwest Petroleum University, Chengdu 610500, China

Abstract

The hydraulic cylinder of the drilling pump is inevitably eroded by drilling fluid during operation, resulting in a decrease in the service life of the hydraulic cylinder. The surface strengthening of the inner chamber of the hydraulic cylinder can effectively improve its service life. However, the specific erosion behavior and surface strengthening effect evaluation of the hydraulic cylinder still need to be studied. To study the erosion behavior of gooseneck pipes in drilling fluid environment and evaluate the surface strengthening effect, this paper establishes a calculation model for the erosion behavior of drilling pump hydraulic cylinder and the surface strengthening of the inner cavity through finite element simulation. Studied the effect of outlet angle of drilling pump hydraulic cylinder on erosion rate and surface strengthening evaluation method. The calculation results show that the erosion rate is the highest near the outlet of the hydraulic cylinder. Reducing the outlet angle appropriately can effectively reduce the erosion rate, with a maximum reduction of 61.1%. After surface strengthening, the inner chamber of the hydraulic cylinder can effectively reduce the maximum deformation displacement, with a maximum reduction of 34.2%. I hope that the research in this article can provide technical support for improving the erosion law and surface strengthening of hydraulic cylinders.

Keywords

Drilling Pump Hydraulic Cylinder; Erosion Behavior; Surface Strengthening; Finite Element Simulation.

1. Introduction

The drilling rig circulation system is an indispensable core piece of equipment in the petroleum drilling process, providing substantial support for the extraction of oil and gas resources. Drilling fluid serves as the lifeblood of the circulation system, primarily functioning to balance or overcome formation pressure in the wellbore and reduce well control risks. As one of the key pressure-bearing components in the drilling circulation system, the drilling pump fluid cylinder mainly converts mechanical energy into hydraulic pressure energy, supplying the necessary power for drilling fluid circulation. During this process, it is inevitably subjected to erosion and damage by the drilling fluid. Surface strengthening offers a promising approach to enhance the erosion resistance of drilling pump fluid cylinders, thereby extending their service life. Consequently, it is essential to understand the erosion behavior of drilling fluid on drilling pump fluid cylinders and the methods for evaluating surface strengthening.

Over recent decades, numerous researchers have investigated the erosion behavior and surface strengthening of critical pressure-bearing components in drilling circulation systems. Song et al.[1] utilized computational fluid dynamics (CFD) software to study gas-solid two-phase flow

ISSN: 2710-0723

wear in 90° elbows. Their results indicate that secondary collision sites are closer to the elbow outlet, often located within the heat-affected zone of the elbow weld, which can intensify wear and even accelerate the propagation of microcracks in the weld's heat-affected zone. Zhou et al.[2] performed numerical simulations based on various fluid velocities, particle mass flow rates, diameters, and fracturing fluid viscosities, summarizing the erosion wear patterns of tee fittings under the combined influence of these factors. Huang et al.[3] employed computational fluid dynamics methods to demonstrate that when the spatial angle ranges between 30° and 45°, maximum erosion concentrates at the intersecting lines of the tee. Tao et al.[4] revealed that for traditional straight-flow-path crosses, regardless of operating conditions, the concentrated erosion area lies along the intersecting lines where the cross sections meet. As the angle increases, the concentrated erosion zone shifts from the intersecting lines and adjacent walls to the cylindrical surface at the outlet end.

Based on the above studies, it is evident that researchers have primarily used numerical simulation methods to investigate the erosion behavior of key pressure-bearing components such as tees, crosses, and elbows, while research on drilling pump fluid cylinders remains a gap. As an essential component of the drilling fluid circulation system, drilling pump fluid cylinders may be subjected to complex working conditions, including pressures ranging from tens to even hundreds of megapascals, high-velocity solid particle impact, and fluid corrosion, making them highly susceptible to erosion damage[5-7]. Therefore, it is necessary to study the erosion behavior of drilling pump fluid cylinders to provide theoretical guidance for evaluating the strength and service life of in-service piping assemblies. Moreover, to improve the service life of drilling pump fluid cylinders, surface strengthening treatment of the cylinder inner cavity is essential, which will effectively prevent failure[8-10]. With the rapid advancement of computer technology, numerical analysis methods have become valuable tools for assessing erosion behavior and the effectiveness of surface strengthening[11]. Hence, this paper employs finite element analysis to investigate the erosion behavior of drilling pump fluid cylinders and the evaluation of inner cavity surface strengthening.

2. Erosion Behavior of the Hydraulic Cylinder of the Drilling Pump

2.1. Erosion Behavior Calculation Model

The hydraulic cylinder of the drilling pump, also known as the valve box, is the most crucial component in the hydraulic end system of the drilling pump. The process of converting mechanical energy into hydraulic energy takes place within the hydraulic cylinder [12-13].

As shown in Figures 1a and 1b, the structural diagram and flow channel model of the fluid cylinder are presented, respectively. In Figure 1b, the blue marking designates the inlet port where drilling fluid enters the cylinder, while the red marking indicates the outlet port where drilling fluid exits. For the interior of the fluid cylinder, which serves as the computational domain for erosion wear study, the region was modeled and meshed using a high-precision octahedral meshing technique to achieve higher mesh quality and computational accuracy, resulting in a well-structured mesh. The model after meshing is shown in Figure 1c. To further observe the internal meshing of the fluid cylinder, a cross-sectional view was created by taking a cross-sectional view from the perspective shown in Figure 1a, as illustrated in Figure 1d.

ISSN: 2710-0723

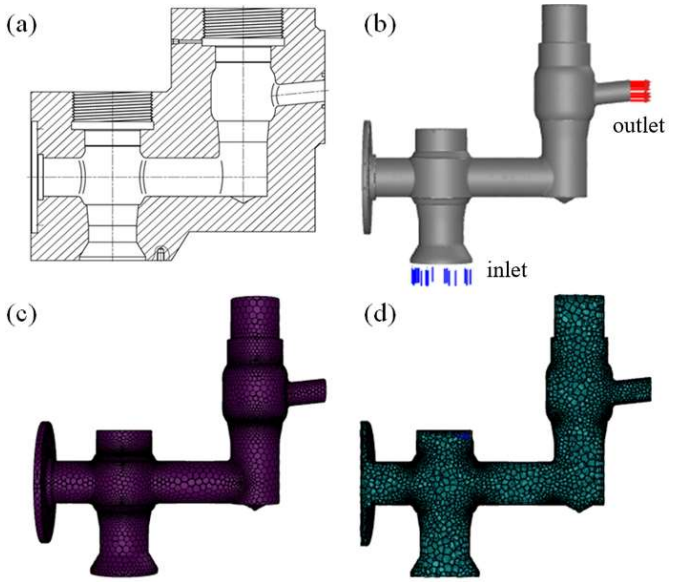

Figure 1. Structure and Model of the Hydraulic Cylinder. (a) is the structural diagram of the hydraulic cylinder, (b) is the flow channel model of the hydraulic cylinder, (c) is the unit model diagram of the hydraulic cylinder, and (d) is the sectional view of the hydraulic cylinder

Based on the operational conditions: a working pressure of 70 MPa, a flow rate of 55 L/s, and the selection of a typical drilling fluid used in Chuanqing Drilling's operations in Sichuan, with a drilling fluid density of 1500 kg/m^3, a plastic viscosity (PV) value of 20 MPa·s, and a commonly used particle diameter of 200 μm (75 mesh) for the drilling fluid.

According to the operational scenario, the total number of cylinders in the drilling pump is five. Under the most severe conditions, only two cylinders are operational. With a total flow rate Q = 55 L/s, the single-cylinder flow rate Q' under the most severe conditions is calculated as follows:

$$Q^{'}=\frac{Q}{n}=27.5L/s \tag{1}$$

In the formula, n represents the number of cylinders, with n = 2. The inflow velocity V of the drilling fluid into the fluid cylinder is:

$$V=\frac{Q^{'}}{\frac{\pi}{4}d^2}=0.86m/s \tag{2}$$

In the formula, d represents the inlet diameter of the fluid cylinder, with d = 203 mm. The actual mass fraction of sand content in the drilling fluid is 0.3%, which meets the requirements of the DPM (Discrete Phase Model) for the discrete phase. The DPM model is employed to simulate the flow characteristics of the dilute dispersed phase in the flow field [14]. Consequently, the mass flow rate P of sand particles within the fluid cylinder is derived from the actual mass fraction of sand content in the drilling fluid as follows:

$$P=Q^{'}\omega\rho=0.125kg/s \tag{3}$$

In the formula, ρ represents the density of the drilling fluid, with ρ = 1500 kg/m^3.

ISSN: 2710-0723

2.2. Flow Field Analysis

Based on the discussion in Section 2, the flow field analysis was conducted with the drilling fluid inflow velocity V set to 0.86 m/s and the mass flow rate P set to 0.125 kg/s. The calculated velocity distribution contour of the drilling fluid inside the fluid cylinder is shown in Figure 2a. As can be observed from Figure 2a, the velocity of the drilling fluid changes during its flow through the cylinder, with particularly noticeable variations occurring at the corners. Furthermore, the flow velocity is relatively low at the inlet of the cylinder and reaches its maximum at the outlet. This may be attributed to the smaller diameter of the outlet compared to the inlet, requiring a higher flow velocity at the outlet to maintain a stable volumetric flow rate. Figure 2b presents the velocity contour of drilling fluid particles. It can be seen from Figure 2b that the particle velocity at the outlet of the cylinder is significantly higher than that at other locations. The results indicate that the maximum particle velocity is predominantly concentrated at the outlet of the fluid cylinder. The high velocity of drilling fluid particles implies greater kinetic energy, which leads to stronger erosive action on the cylinder and is likely to cause erosion damage to the inner wall of the fluid cylinder.

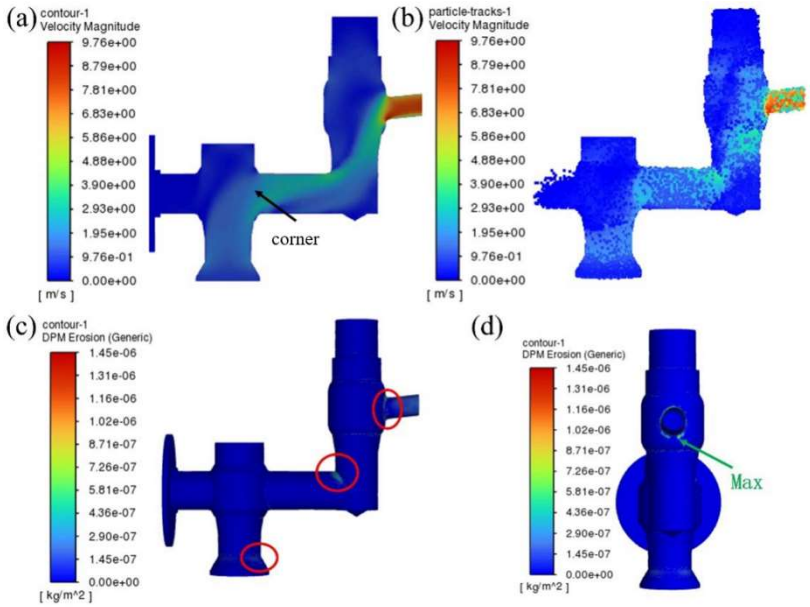

Figure 2. (a) shows the contour plot of the flow velocity distribution of drilling fluid in the hydraulic cylinder, (b) shows the contour plot of the particle velocity of drilling fluid, and (c) and (d) show the contour plots of the overall erosion rate of the hydraulic cylinder. The red box represents the chamfered area with a high erosion rate

To further investigate the erosion behavior of the fluid cylinder in a drilling fluid environment, the overall erosion rate contour of the cylinder was calculated, as shown in Figures 2c and 2d. From Figure 2c, it can be observed that during the flow of drilling fluid inside the cylinder, erosion primarily occurs at the chamfered corners (indicated by the red boxed area in Figure 2c). This is likely due to the high-speed impact of particles in the drilling fluid against the wall when the flow direction changes. Figure 2d illustrates the region with the highest overall erosion rate in the cylinder, which is near the outlet. This can be attributed to the maximum velocity of drilling fluid particles at the outlet (Figure 2b), where their greater kinetic energy results in stronger impacts and consequently the highest erosion rate.

ISSN: 2710-0723

2.3. The Impact of the Exit Angle on the Erosion Rate

Based on the flow field analysis of the fluid cylinder, it is observed that the drilling fluid particles attain the highest velocity at the outlet of the cylinder, leading to a significant erosion rate at this location. This may cause the inner wall to be eroded and damaged earliest. Therefore, it is necessary to conduct further research on the structure of the cylinder outlet to explore whether changes in the cylinder structure can reduce the erosion rate and thereby extend the service life of the cylinder. For this purpose, the influence of the outlet angle of the cylinder on the erosion rate was investigated.

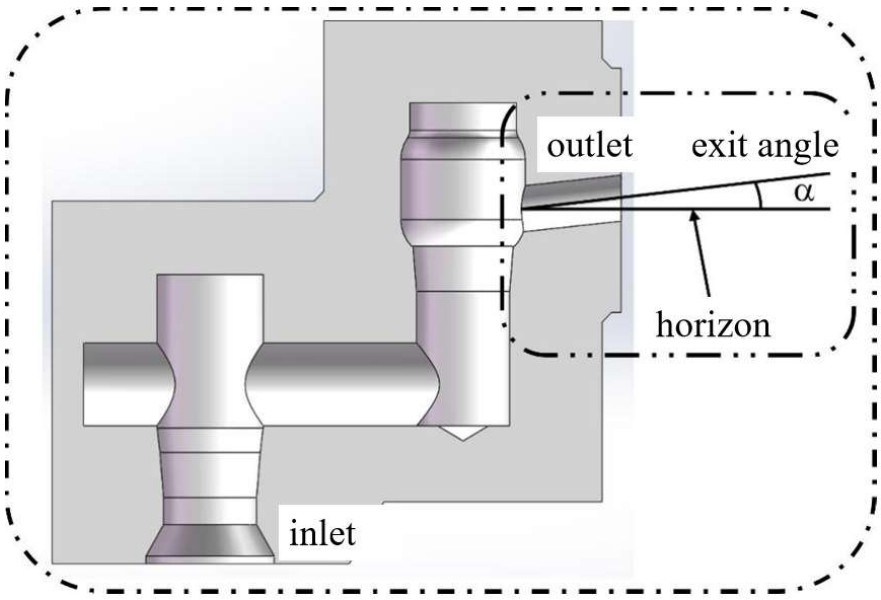

Figure 3. Schematic diagram of the outlet angle of the hydraulic cylinder

As shown in Figure 3, we have defined the outlet angle. The outlet angle refers to the inclination angle of the pipeline at the outlet of the hydraulic cylinder, and the default outlet angle of the hydraulic cylinder is generally 6°.

We established five sets of different outlet angles (θ = 0°, 2°, 4°, 6°, and 8°, where 6° is the initial angle), representing conditions of both increased and decreased outlet angles, and performed computational simulations. The erosion rate contour maps were output and the erosion rates were calculated, as shown in Figure 4. From the relationship between the maximum erosion rate and the outlet angle (Figure 4f), it can be seen that as the outlet angle increases from 0° to 4°, the maximum erosion rate gradually decreases. However, when the outlet angle increases from 4° to 8°, the maximum erosion rate progressively increases. The minimum maximum erosion rate occurs at an outlet angle of 4°. The results show that reducing the outlet angle from 6° to 4° can effectively lower the maximum erosion rate (by approximately 61.1%), which will significantly reduce the probability of erosion damage at the cylinder outlet. Furthermore, as seen in Figure 4c, when the outlet angle is 4°, the maximum erosion rate occurs at the lower part of the outlet, implying that the lower part of the outlet may experience damage earlier under the erosive action of the drilling fluid. When the outlet angle is 8° (Figure 4e), the maximum erosion rate appears at the upper part of the outlet. The results indicate that, based on the initial outlet angle of 6°, increasing the outlet angle not only leads to a higher maximum erosion rate but also changes the location where the maximum erosion rate occurs.

ISSN: 2710-0723

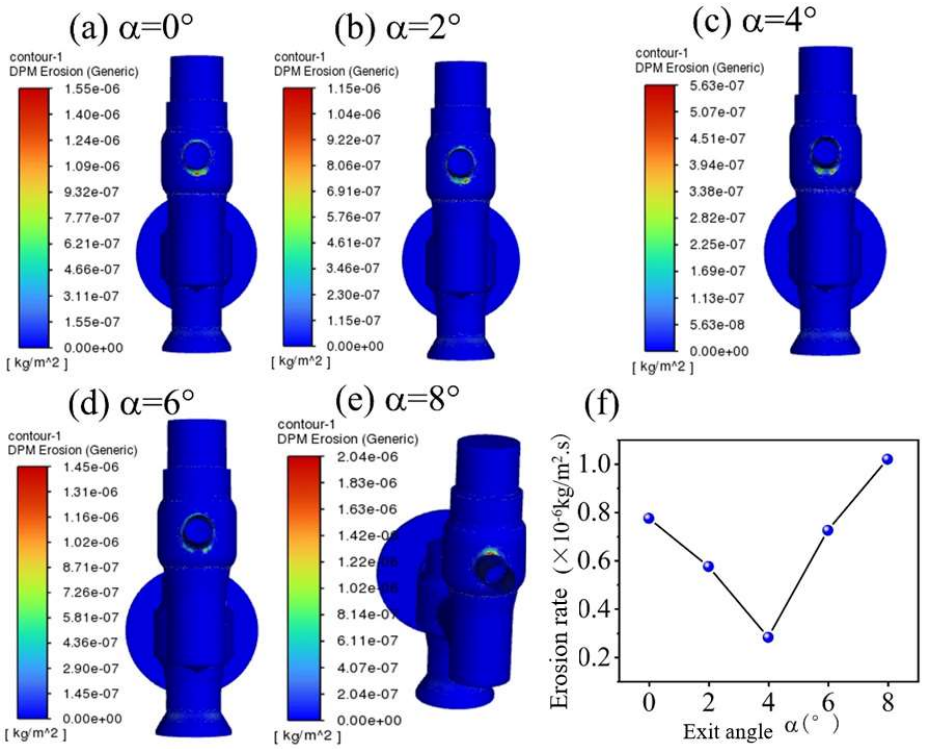

Figure 4. Erosion rate and erosion velocity at different exit angles. (a) to (e) are contour plots of erosion rate, and (f) shows the relationship between maximum erosion velocity and exit angle

3. Surface Strengthening of the Inner Cavity of the Drilling Pump Cylinder

3.1. Stress Analysis of the Inner Cavity Surface

During the operation of the drilling pump fluid cylinder, the cylinder primarily bears alternating loads imposed by the drilling fluid, and the variation in load is synchronized with the changes in drilling fluid pressure. The drilling fluid pressure in the cylinder is divided into suction pressure p_1, discharge pressure p_2, and working chamber pressure pc. The load borne by the cylinder during operation is the working chamber pressure pc, and the working chamber pressure pc is jointly influenced by both the suction pressure p1 and the discharge pressure p2.

The suction pressure p1 is defined as the pressure at the suction port of the hydraulic end of the cylinder converted to the reference plane of the cylinder. The calculation formula is as follows:

$$p_1 = p_1' - \frac{\gamma h_1}{10} \tag{4}$$

In the formula, p_1 represents the suction pressure (absolute) in kgf/cm^2; p_1' denotes the inlet pressure of the fluid cylinder (absolute) in kgf/cm^2; γ stands for the specific weight of the drilling fluid in kgf/l; and h_1 indicates the vertical distance from the cylinder inlet to the cylinder reference plane in meters.

The actual suction pressure p_1 during cylinder operation depends on the pipeline characteristics and is related to the minimum cavitation pressure of the cylinder. The calculation formula is as follows:

$$\frac{10p_1}{\gamma} = \frac{10p_s}{\gamma} - h_s - h_{a1} - h_{f1} - \frac{v_1^2}{2g} \tag{5}$$

ISSN: 2710-0723

In the formula, p_s represents the pressure (absolute) on the liquid surface in the suction vessel (kgf/cm^2); hs denotes the vertical distance from the liquid surface in the suction vessel to the reference plane of the cylinder; ha_1 stands for the acceleration head of the liquid in the suction pipe; h_{f_1} indicates the friction head loss of the liquid in the suction pipe; v_1 represents the flow velocity of the liquid in the suction pipeline (flow velocity at the cylinder inlet) (m/s); and g is the acceleration due to gravity.

The discharge pressure p_2 is defined as the pressure at the discharge port of the cylinder's hydraulic end converted to the reference plane of the cylinder. The calculation formula is as follows:

$$p_2=p_2^{'}+\frac{\gamma h_2}{10} \tag{6}$$

In the formula, p_2 represents the discharge pressure (absolute) in kgf/cm^2; p_2' denotes the outlet pressure of the cylinder (absolute) in kgf/cm^2; and h_2 indicates the vertical distance from the cylinder outlet to the cylinder reference plane in meters.

Similar to the suction pressure p_1, the discharge pressure p_2 is not an inherent property of the cylinder and also depends on the pipeline characteristics. The calculation formula for the actual discharge pressure p_2 during cylinder operation is as follows:

$$\frac{10p_2}{\gamma}=\frac{10p_d}{\gamma}-h_d-h_{a2}-h_{f2}-\frac{v_2^2}{2g} \tag{7}$$

In the formula, p_d represents the pressure (absolute) on the liquid surface in the discharge vessel (kgf/cm^2); h_d denotes the vertical distance from the liquid surface in the discharge vessel to the reference plane of the cylinder (m); h_{a_2} stands for the acceleration head of the liquid in the discharge pipe; h_{f_2} indicates the friction head loss of the liquid in the discharge pipe; and v_2 represents the flow velocity of the liquid in the discharge pipeline (flow velocity at the cylinder outlet) (m/s).

During the suction stroke of the cylinder, the pressure in the working chamber is as follows:

$$\frac{10p_{c1}}{\gamma}=\frac{10p_1}{\gamma}-\left(h_{v1}+h_{ac1}+h_{fc1}+\frac{u^2-v_1^2}{2g}\right) \tag{8}$$

In the formula, p_{c_1} represents the pressure in the working chamber during the suction stroke (kgf/cm^2); h_{v_1} denotes the resistance of the suction valve (N); h_{ac_1} stands for the acceleration head of the drilling fluid in the working chamber during the suction stroke; h_{fc_1} indicates the friction head loss in the working chamber during the suction stroke; u represents the displacement velocity of the piston (m/s); and v_1 denotes the flow velocity in the suction pipe (m/s).

During the discharge stroke of the cylinder, the pressure in the working chamber is as follows:

$$\frac{10p_{c2}}{\gamma}=\frac{10p_2}{\gamma}+\left(h_{v2}+h_{ac2}+h_{fc2}-\frac{u^2-v_2^2}{2g}\right) \tag{9}$$

In the formula, p_{c_2} represents the pressure in the working chamber during the discharge stroke (kgf/cm^2); h_{v_2} denotes the resistance of the discharge valve (N); h_{ac_2} stands for the acceleration head of the drilling fluid in the working chamber during the discharge stroke; h_{fc_2} indicates the

ISSN: 2710-0723

friction head loss in the working chamber during the discharge stroke; and v_2 represents the flow velocity in the discharge pipe (m/s).

Substituting formula (5) into formula (8) yields the calculation formula for the pressure in the working chamber during the suction stroke:

$$\frac{10p_{c1}}{\gamma} = \frac{10p_s}{\gamma} - h_s - h_{a1} - h_{f1} - h_{v1} - h_{ac1} - h_{fc1} - \frac{u^2}{2g} \tag{10}$$

Substituting formula (7) into formula (9) yields the calculation formula for the pressure in the working chamber during the discharge stroke:

$$\frac{10p_{c2}}{\gamma} = \frac{10p_d}{\gamma} + h_d + h_{a2} + h_{f2} + h_{v2} + h_{ac2} + h_{fc2} - \frac{u^2}{2g} \tag{11}$$

3.2. Calculation Model for Internal Cavity Surface Strengthening

As shown in Figure 5, the computational model for surface reinforcement of the inner cavity of the drilling pump fluid cylinder is presented. Figure 5a displays the results of the mesh generation. The meshing was performed using a tetrahedron-dominated approach [15]. After meshing, the maximum cell size obtained was 12 mm, with a node count of 1,682,903 and a cell count of 1,213,776. The boundary conditions were set according to the working conditions of the fluid cylinder, as detailed below:

(1) A gravitational acceleration of g = 9.80 m/s^2 was applied in the vertically downward direction.

(2) Based on the installation method of the cylinder, full constraints (no degrees of freedom) were applied to the upper and lower outer surfaces of the cylinder.

(3) A symmetry constraint was applied to the cut surface obtained by sectioning the cylinder along the central axis of the inner cavity.

(4) According to the working state of the cylinder during the discharge stroke, a surface pressure of 70 MPa was applied to the relevant face (the red face in Figure 5b).

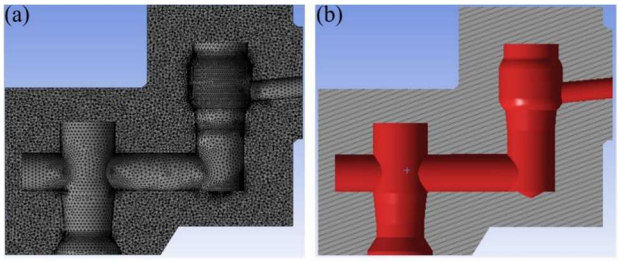

Figure 5. Grid division and load application of the drilling pump cylinder. (a) shows the grid division results, and (b) shows the load application surface

Table 1. Material properties of the hydraulic cylinder cavity after surface strengthening

	30CrNi3MoV (part 1)	30CrNi3MoV_1 (part 2)	30CrNi3MoV_2 (part 3)	30CrNi3MoV_3 (part 4)
Density/(kg·m^{-3})	7890	7890	7890	7890
Young's modulus/(GPa)	211	240	280	320
Poisson's ratio	0.30	0.28	0.26	0.24
Bulk modulus/(GPa)	175.8	181.8	199.4	205.1
shear modulus/(GPa)	81.1	93.8	111.1	129.0

ISSN: 2710-0723

It is noteworthy that, considering the surface pressure on the inner cavity of the cylinder is unstable under actual drilling fluid action, an alternating load of 70 MPa was applied to the inner cavity. To represent the inner cavity surface treated with different surface strengthening methods, parameters such as Young's modulus, Poisson's ratio, bulk modulus, and shear modulus of the material were modified (30CrNi3MoV steel is a typical material used for manufacturing cylinders. According to relevant data, the Young's modulus of surface-strengthened 30CrNi3MoV steel increases while the Poisson's ratio decreases. Therefore, four groups of models with increased Young's modulus and decreased Poisson's ratio were established), as shown in Table 1. It is important to note that the surface-strengthened 30CrNi3MoV steel samples are labeled as Group 1, Group 2, Group 3, and Group 4, respectively. Group 1 serves as the control group, while Groups 2, 3, and 4 are the experimental groups.

3.3. Evaluation of Internal Cavity Surface Strengthening

To evaluate the strengthening effect of the drilling pump's inner cavity, deformation displacement was selected for study. Analyzing the magnitude of deformation displacement provides an intuitive understanding of the effectiveness of surface strengthening—specifically, whether it can reduce deformation displacement in the inner cavity to achieve the desired strengthening outcome. Additionally, analyzing the deformation displacement helps identify the areas of the cylinder where deformation is most severe, offering theoretical guidance for the practical processing and strengthening of the inner cavity surface. Based on the above discussion, deformation displacement contour plots of the cylinder inner cavity for different groups were visualized, as shown in Figure 6.

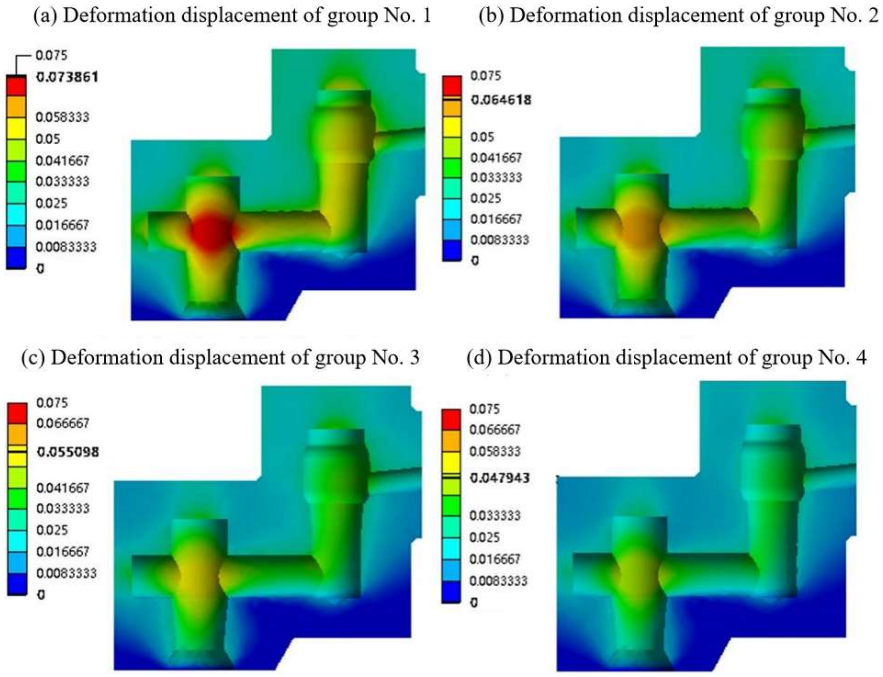

Figure 6. Cloud chart of deformation displacement in the inner cavity of the drilling pump cylinder

Figure 6 shows the deformation displacement contours of the control group (Group 1) and the experimental groups (Groups 2, 3, and 4) under an inner cavity pressure of 70 MPa. It can be observed that Group 1 exhibits the largest deformation displacement, followed by Group 2, then Group 3, while Group 4 shows the smallest deformation displacement. The maximum deformation displacement for all groups appears to occur in the left cavity. The results indicate that surface strengthening of the drilling pump cylinder inner cavity can effectively reduce

ISSN: 2710-0723

deformation displacement, thereby lowering the risk of material failure in the inner cavity. Furthermore, the region of maximum deformation displacement is mainly concentrated at the first corner near the cylinder inlet. In practical strengthening processes, additional reinforcement of this area may be considered.

To further investigate the deformation displacement across different groups, the trend of maximum deformation displacement was calculated, as shown in Figure 7. Group 1 has the largest maximum deformation displacement value of 0.073 mm, while Group 4 has the smallest value of 0.048 mm. The maximum deformation displacement values for Groups 2 and 3 are 0.065 mm and 0.055 mm, respectively. The above analysis demonstrates that surface strengthening of the drilling pump cylinder can effectively reduce the maximum deformation displacement. Compared with the control group (Group 1), the maximum reduction reaches 34.2% (Group 4), which will significantly decrease the risk of severe deformation in the cylinder inner cavity and thereby extend its service life.

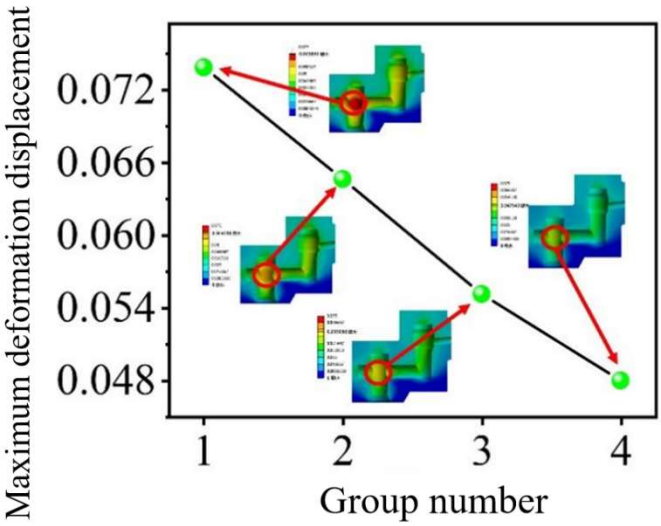

Figure 7. Maximum deformation displacement of the drilling pump cylinder

4. Conclusion

(1) This paper investigates the erosion behavior of the drilling pump fluid cylinder and evaluates the surface strengthening of its inner cavity through finite element simulation. Analysis of the internal drilling fluid flow field indicates that the erosion rate is highest near the outlet of the cylinder, where the velocity of drilling fluid particles is also greatest.

(2) By varying the outlet angle of the cylinder, it was found that an optimal outlet angle exists. Specifically, when the outlet angle is 4°, the erosion rate reaches its minimum value-a reduction of 61.1% compared to the initial angle.

(3) Surface strengthening of the inner cavity effectively reduces the maximum deformation displacement, with a maximum reduction of 34.2%. This demonstrates that the strengthened inner cavity can better resist risks induced by significant deformation, thereby extending the service life of the cylinder.

References

[1] SONG Xiaoqin, HUANG Shiwei, ZHU Shanshan. Study on the Wear of Gas Solid Two Phase Flow in a 90° Bend[J]. Drilling & Production Technology, 2015, 38(6): 56-59.

[2] ZHOU Fang, QIAN Yubao, REN Yilang, et al. Erosion Wear Analysis of Shale Gas Fracturing Tee Manifold[J]. Science Technology and Engineering, 2023, 23(6): 2396-2402.

ISSN: 2710-0723

[3] HUANG Huabao, QIAN Yubao, GUO Xutao, et al. Numerical Simulation of High Pressure Pipe Sink Erosion and Wear Based on DDPM model[J]. Science Technology and Engineering, 2023, 23(26): 11195-11201.

[4] TAO Wenjie, LI Meiqiu, XING Lili, et al. Design and analysis of four-way flow channel undersolid-liquid erosion[J]. Science Technology and Engineering, 2022, 22(15): 6092-6098.

[5] XU Jing. Method and Practice of lmproving Comprehensive Technical Performance of High Pressure Drilling Pump[J]. Petrochemical Industry Technology, 2023, 30(02): 61-63.

[6] WANG Jiasong, LV Xiaofeng, RAO Jianguo, et al. Common Failure Forms Analysis of Hydraulic Cylinder in Drilling Mud Pump[J]. Mechanical Engineering & Automation, 2022, (06): 220-221.

[7] LV Hao. Cracking Failure Analysis of Hydraulic Cylinder in Drilling Mud Pump[J]. Hot Working Technology, 2019, 48(07): 255-258+261.

[8] XU Zhigang, YANG Yang, YANG Zhongna, et al. Effect of surface strengthening on microstructure and properties of C17200 beryllium bronze substrate for logging while drilling equipment[J]. Heat Treatment of Metals, 2023, 48(06): 107-113.

[9] YANG Yuhui, WEI Xin, LONG Zhili, et al. Review on Fatigue Evolution of Surface State Characteristics of Deformation Strengthened Metal Materials[J]. Surface Technology, 2023, 52(06): 112-125+234.

[10] HE Yunyi, YANG Tinghan, JIANG Wei, et al. Enhancement of water-annular heavy oil transportation by superhydrophilic surface[J]. Oil & Gas Storage and Transportation, 2023, 1-17.

[11] XU Dingjiang, JIANG Yuan, YANG Yunshan, ea al. Lab Experiment and Numerical Modeling of Sulfur-resisting Downhole Choke Under 105 MPa Differential Pressure[J]. Drilling & Production Technology, 2021, 44(4): 81-85.

[12] TAN Liqin, MA Guangshe, JIANG Xiaogang, et al. Lightweight Research of F-series Drilling Pumps[J]. Mechanical Engineer, 2018, (06): 69-71.

[13] HUANG Wei. Discussion on the Processing Technology of the Valve Seat Hole in the Hydraulic Cylinder of the W Series Drilling Pump[J].Internal Combustion Engine & Parts, 2020, (10): 58-59.

[14] WANG Zhiliang, WU Zhenhua, WANG Zhensong, et al. Simulation Analysis of 90° Curved Flow Channel Erosion in Jet Pump Based on CFD-DPM[J]. Machine Tool & Hydraulics, 2023, 51(14): 174-181+232.

[15] WANG Zhiliang, WU Zhenhua, WANG Zhensong, et al. Simulation Analysis of 90° Curved Flow Channel Erosion in Jet Pump Based on CFD-DPM[J]. Machine Tool & Hydraulics, 2023, 51(14): 174-181+232.

[16] LIU Tiantian, ZHENG Peng, LENG Juelin, et al. Local Tetrahedra Mesh Remeshing for Adaptive Computation[J]. Journal of Jilin University(Science Edition), 2021, 59(06), 1461-1468.